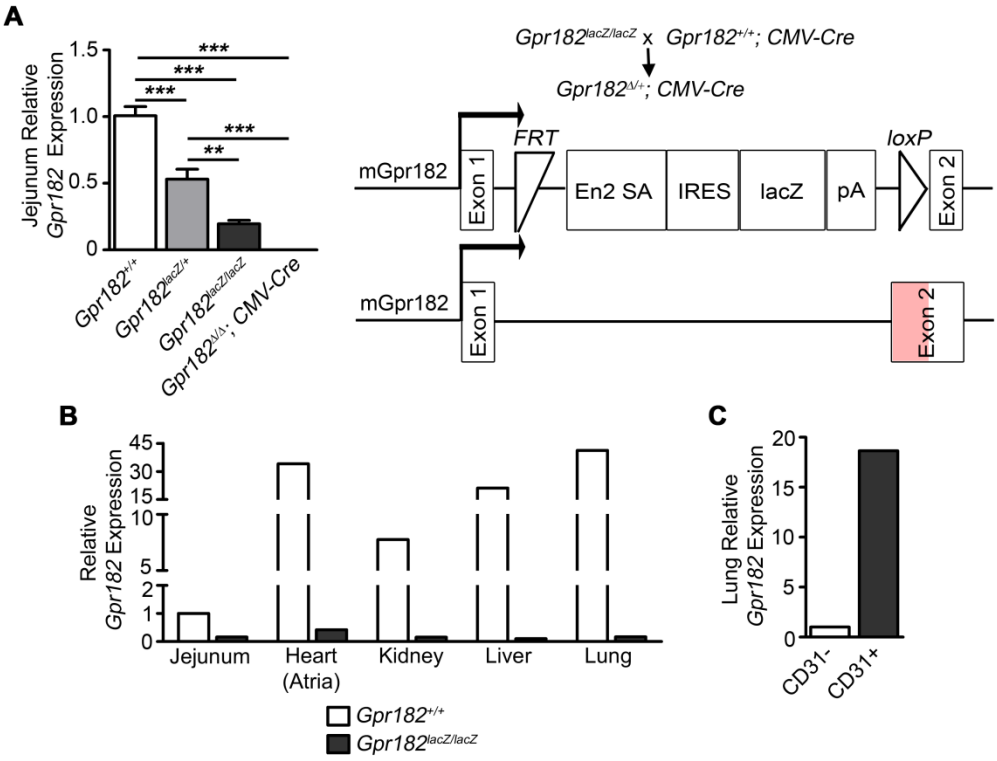

Supplemental Figure 1: Relative murine *Gpr182* expression in numerous adult tissues. **(A)** Relative *Gpr182* expression in adult jejunum from *Gpr182*$^{+/+}$, *Gpr182*$^{lacZ/+}$, *Gpr182*$^{lacZ/lacZ}$, *Gpr182*$^{\Delta/\Delta}$*; CMV-Cre* mice. Biological n = 3-5 mice per genotype. The generation of the *Gpr182*$^{\Delta/+}$*; CMV-Cre* mouse model by crossing *Gpr182*$^{lacZ/lacZ}$ mice to *Gpr182*$^{+/+}$*; CMV-Cre* mice. The Gpr182 protein coding region is shaded pink. **(B)** Relative *Gpr182* expression in whole jejunum, atria, kidney, liver, and lung from adult *Gpr182*$^{+/+}$ and *Gpr182*$^{lacZ/lacZ}$ mice. Data normalized to *Gpr182*$^{+/+}$ jejunum, *Gapdh,* and *18S*. **(C)** Relative *Gpr182* expression in CD31- and CD31+ endothelial cells isolated from adult *Gpr182*$^{+/+}$ lung. Expression normalized to CD31- and *Gapdh*. Significance was determined by 1-way ANOVA with Tukey's Multiple Comparison Test.

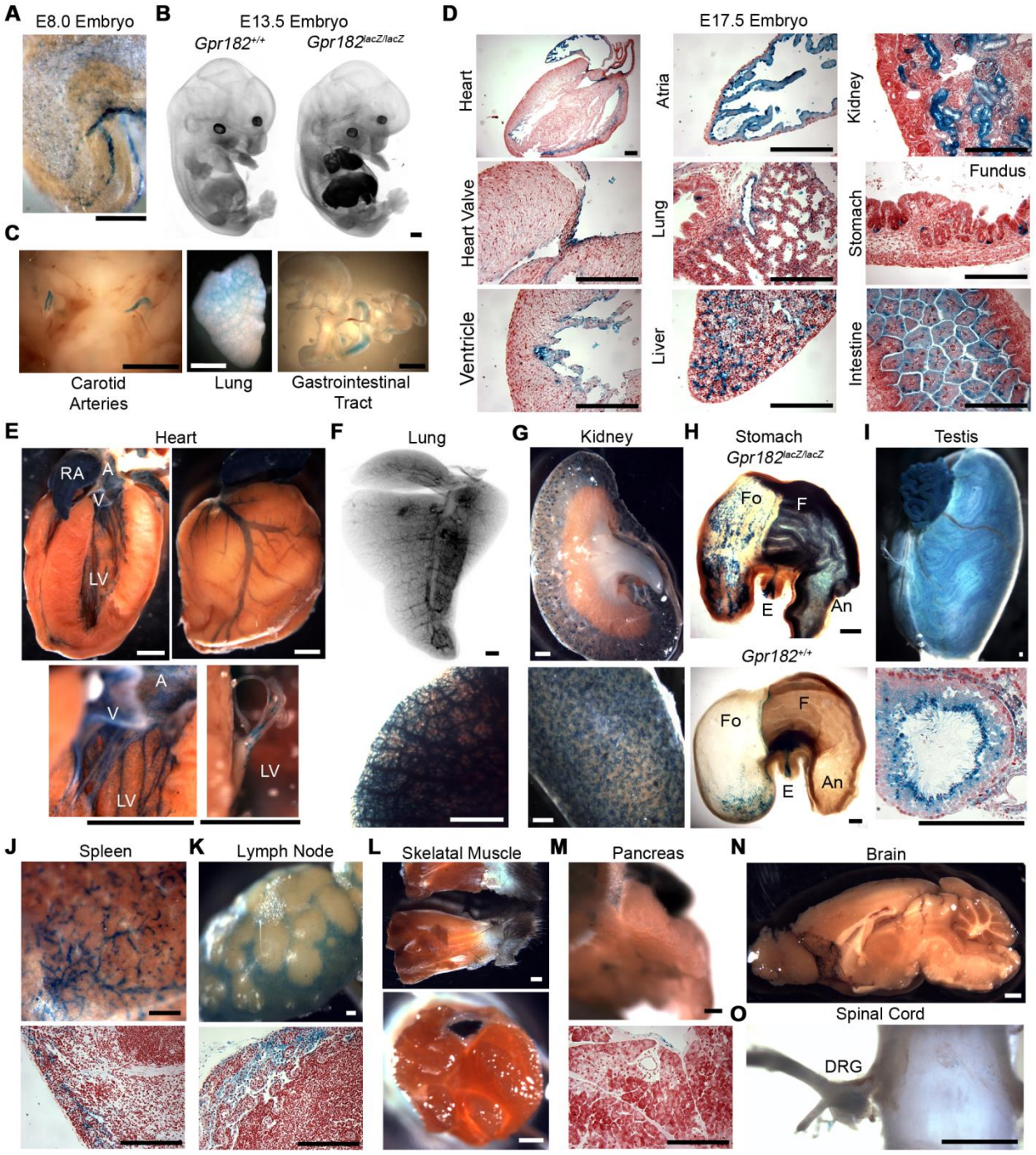

Supplemental Figure 2: Additional murine *Gpr182* expression during development and adulthood. Representative whole mount X-gal staining of *Gpr182*$^{lacz/lacZ}$ tissue during development **(A-D)** and adulthood **(E-O)**. X-gal staining **(A)** of an E8 embryo, **(B)** OPT, and **(C)** microdissected of an E13.5 embryo. **(D)** *Gpr182 lacZ* in heart, lung, liver, kidney, stomach, and small intestine of an E17.5 embryo. Representative images of X-gal staining in adult heart **(E)**, lung OPT **(F)**, kidney **(G)**, stomach **(H)**, testis **(I)**, spleen **(J)**, mesenteric lymph node **(K)**, hindlimb skeletal muscle **(L)**, pancreas **(M)**, brain **(N)**, and spinal cord **(O)**. **(E)** LV, left ventricle; RA, right atria; V, cardiac valve; A, aorta; **(H)** E, esophagus; Fo, forestomach; F, fundus; An,

antrum; **(O)** DRG, dorsal root ganglia. X-gal sections were counterstained with Neutral Red **(D, I-K, M)**. Scale bars represent 200 μm (**A**,**D**,**I**-**K**,**M**) or 1 mm (**B**-**C**,**E**-**H**,**L**,**N**,**O**).

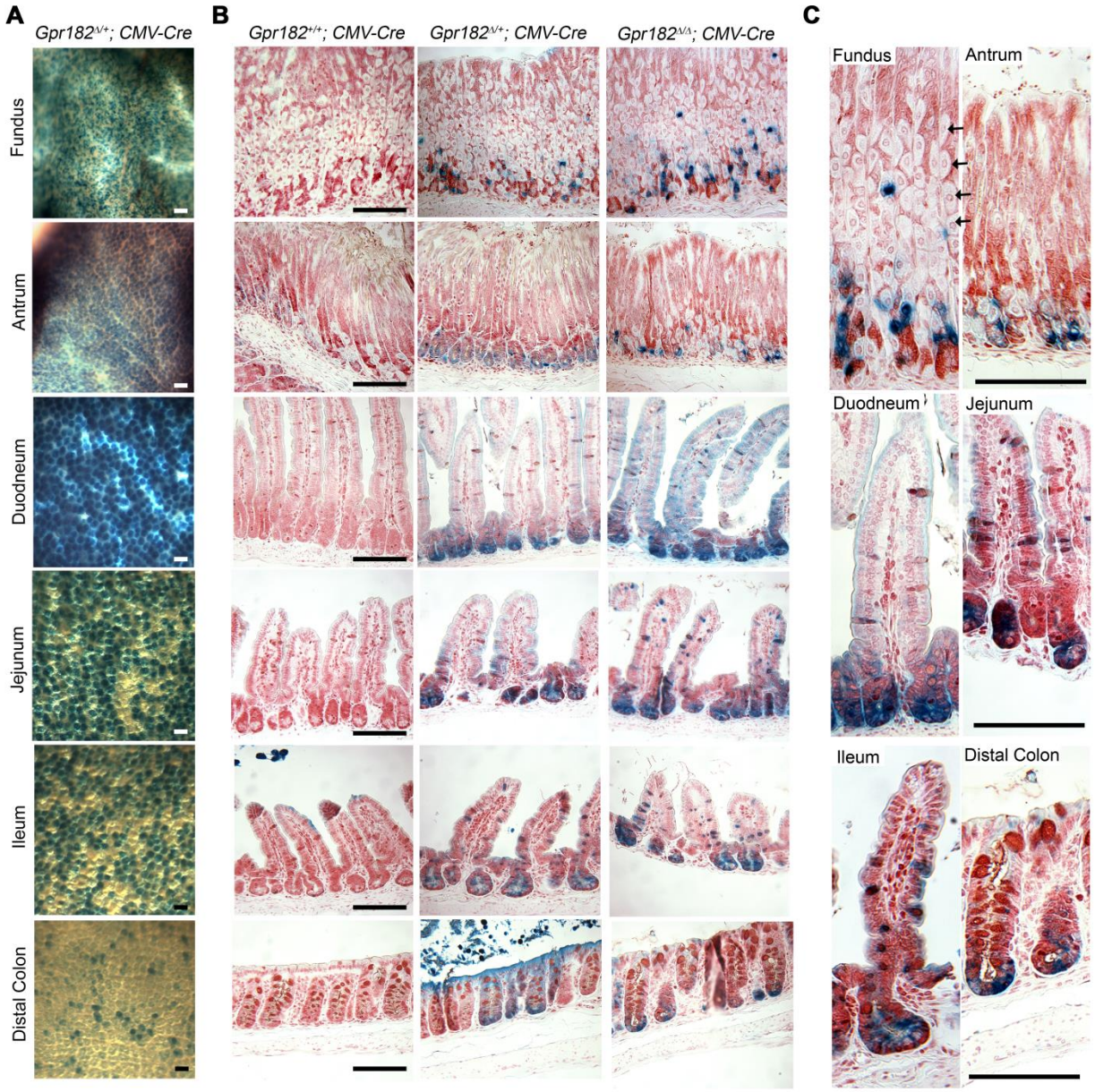

Supplemental Figure 3: *Gpr182* knockout does not alter X-gal expression pattern or cell markers. (A) Representative whole mount X-gal stained stomach, small intestine, and colon of adult *Gpr182*$^{\Delta/+}$*; CMV-Cre*+ mice. **(B)** Representative cross-sections from whole mount X-gal stained stomach, small intestine, and colon from *Gpr182*$^{+/+}$, *Gpr182*$^{\Delta/+}$, *Gpr182*$^{\Delta/\Delta}$ mice. **(C)** Higher magnification of X-gal stained stomach, small intestine, and colons from *Gpr182*$^{\Delta/+}$ or *Gpr182*$^{\Delta/\Delta}$ mice. Arrows mark parietal cells identified by histology. Scale bars represent 100 μm.

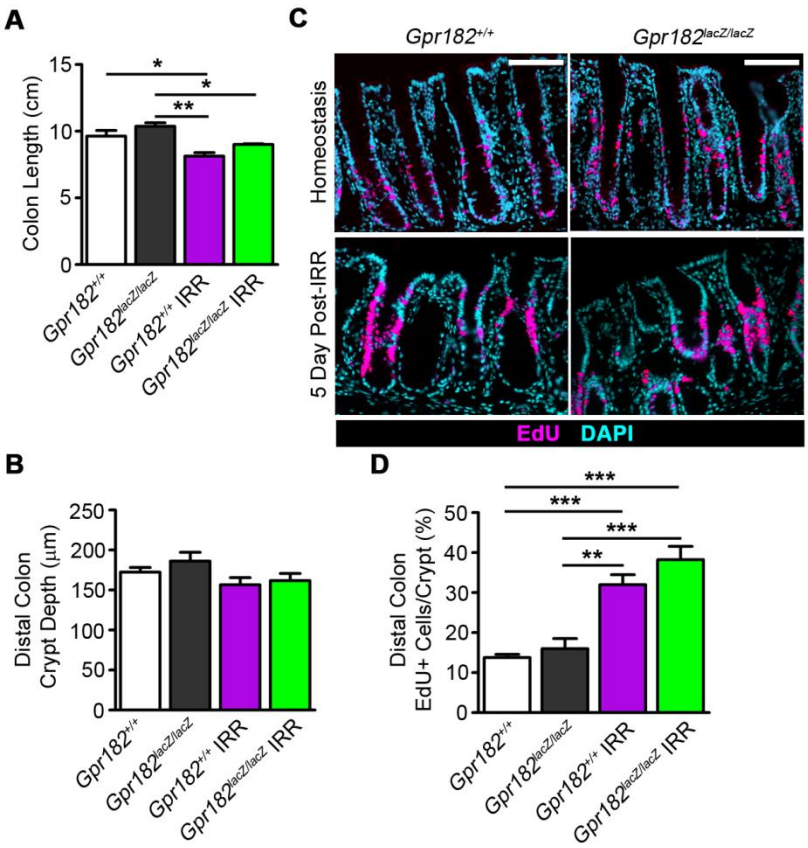

Supplemental Figure 4: *Gpr182* knockdown does not significantly alter homeostatic or regenerative proliferation in the distal colon. (A) Colon length from adult *Gpr182*$^{+/+}$ and *Gpr182*$^{lacZ/lacZ}$ mice both basally and 5d following 14 Gy irradiation (IRR). **(B)** Histological quantification of distal colon crypt depth between *Gpr182* genotypes. **(C)** Representative images and **(D)** EdU incorporation quantification of distal colon proliferation between *Gpr182*$^{+/+}$ and *Gpr182*$^{lacZ/lacZ}$ animals. Biological n = 3-5 mice per genotype. Scale bars represent 100 μm. Significance was determined either by the 1-way ANOVA with Tukey's Multiple Comparison Test.

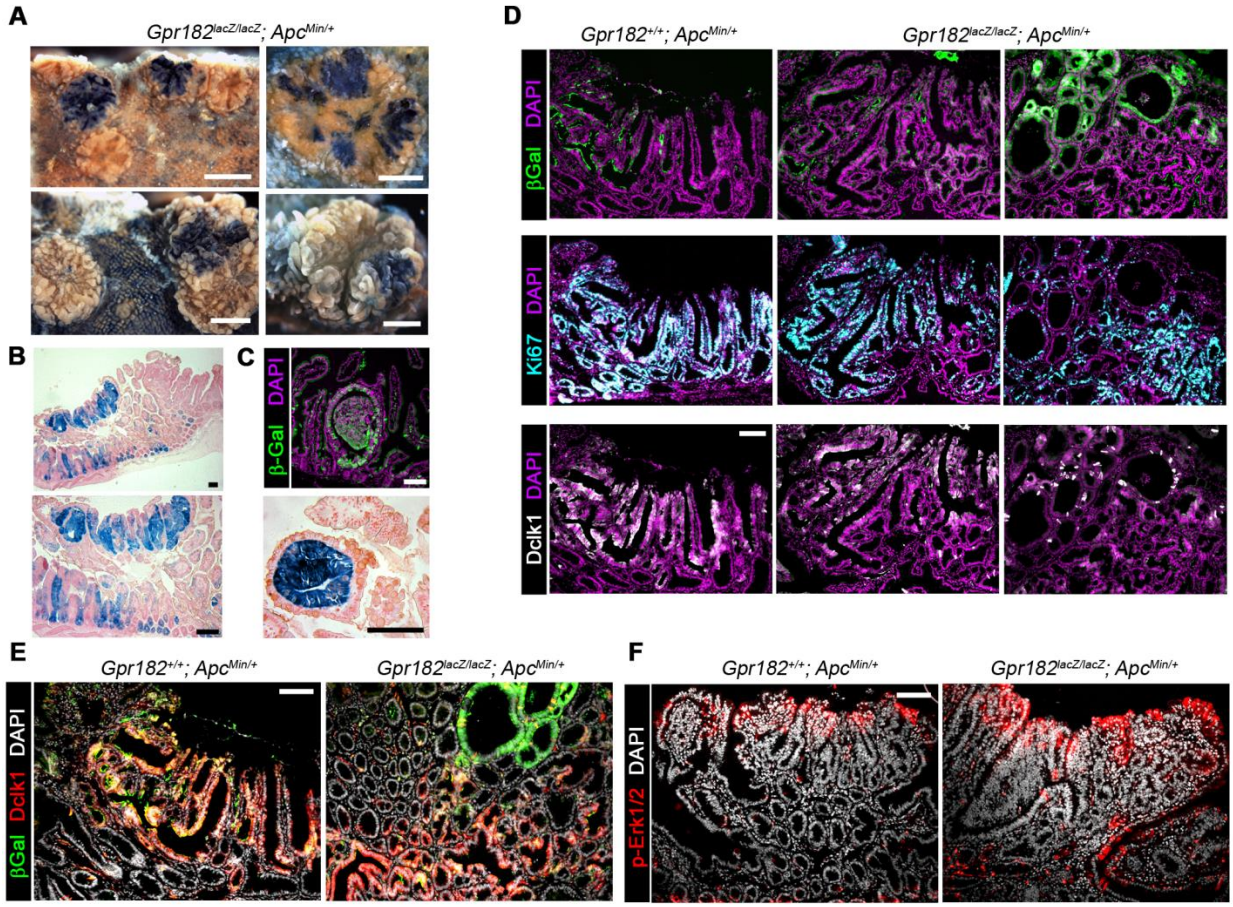

Supplemental Figure 5: Mosaic *Gpr182* staining within polyps corresponded to polyp proliferation heterogeneity. Macroscopic **(A)** and histologic **(B-D)** X-gal staining of *Gpr182*$^{lacZ/lacZ}$*; Apc*$^{Min/+}$ polyps. **(D)** Serial sections stained with β-gal (green), Ki67 (blue), Dclk1 (white), and DAPI (magenta) in *Gpr182*$^{+/+}$ and *Gpr182*$^{lacZ/lacZ}$ polyps. **(E)** Costain β-gal (green), Dclk1 (red), and DAPI (white) polyp from *Gpr182*$^{+/+}$ and *Gpr182*$^{lacZ/lacZ}$ mice. **(F)** Phospho-Erk1/2 (red) staining in polyps from *Gpr182*$^{+/+}$ and *Gpr182*$^{lacZ/lacZ}$ *Apc*$^{Min/+}$ mice. Scale bars represent 1 mm **(A)** and 100 μm **(B-F)**.

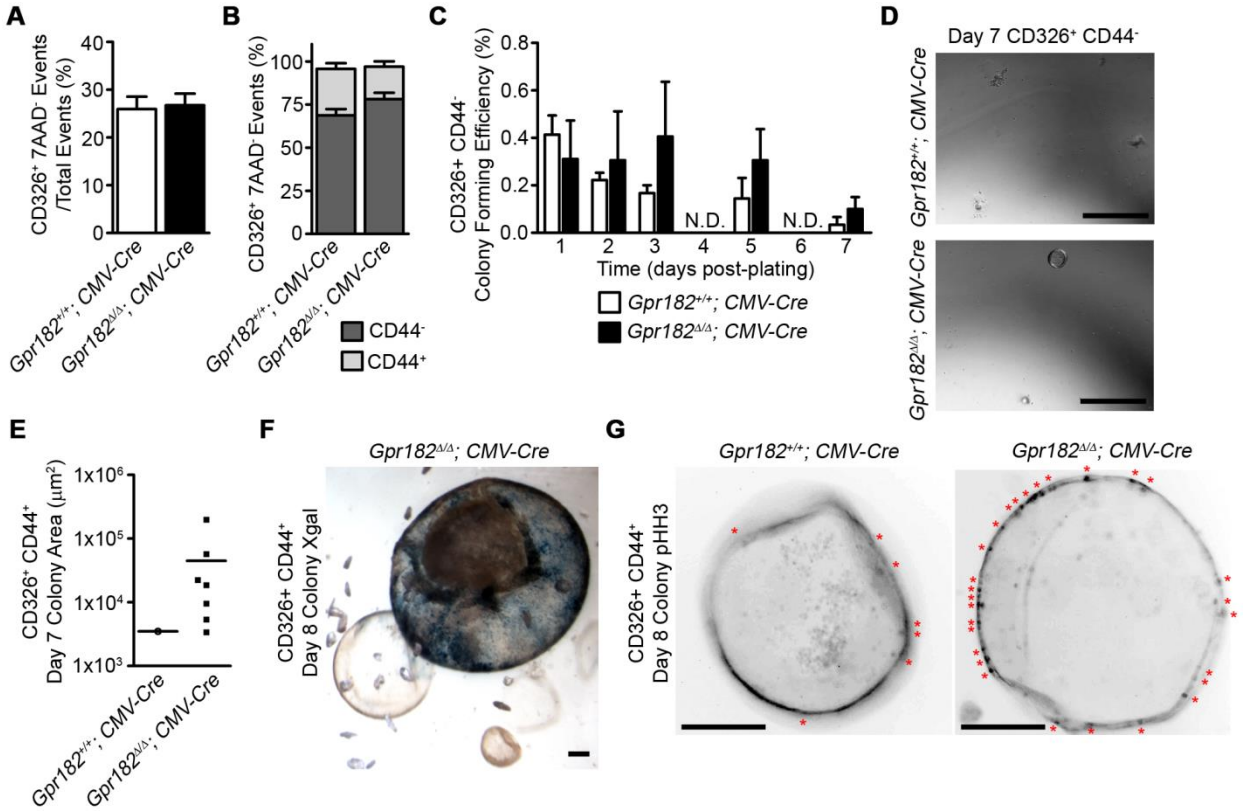

Supplemental Figure 6: Loss of *Gpr182* does not significantly increase the growth efficiency of single CD44- epithelial cells ex vivo. **(A)** Percentage of viable CD326$^+$ epithelial cells from *Gpr182$^{+/+}$; CMV-Cre* and *Gpr182$^{\Delta/\Delta}$; CMV-Cre* jejunum. **(B)** Percentage of viable CD326$^+$ epithelium that are CD44$^+$ and CD44$^-$. **(C)** Growth efficiency of single CD326$^+$CD44$^-$ cells isolated from *Gpr182$^{+/+}$; CMV-Cre* and *Gpr182$^{\Delta/\Delta}$; CMV-Cre* jejunum cultured for 7 d ex vivo. One thousand CD326$^+$CD44$^-$ cells were initially plated in triplicate per mouse. **(D)** Representative images of CD326$^+$CD44$^-$ organoids following 7 d in culture. **(E)** Area quantification of CD326$^+$CD44$^-$ colonies following 7 d in culture. Representative images of **(F)** X-gal or **(G)** phospho-histone H3 (red asterisk) stained organoids from CD326$^+$CD44$^+$ colonies from *Gpr182$^{+/+}$; CMV-Cre* and *Gpr182$^{\Delta/\Delta}$; CMV-Cre* following 8 d in culture. Scale bars represent 500 μm **(D)** and 100 μm **(F-G)**. Biological n = 3 mice. Significance was determined by two-tailed Student's T-test.

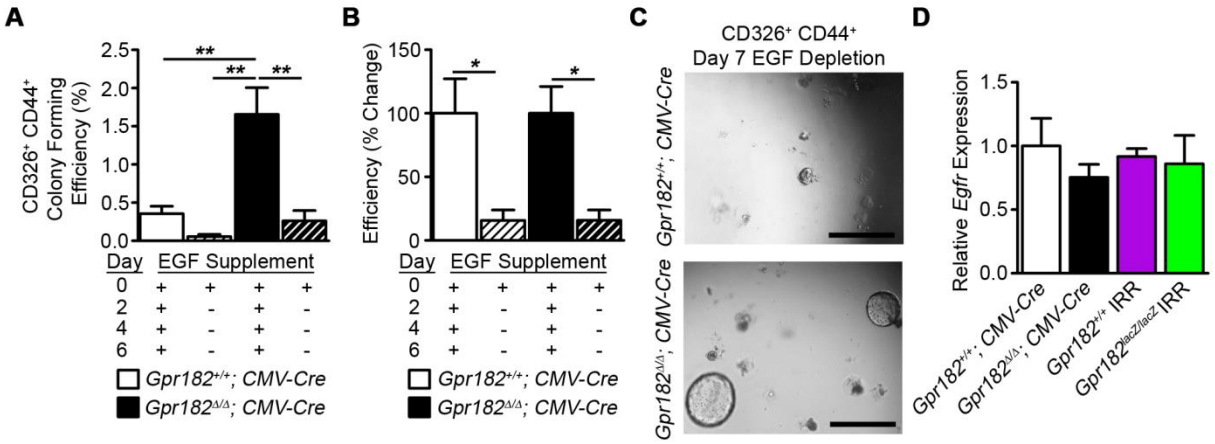

Supplemental Figure 7: Single CD326$^+$CD44$^+$ cells require exogenous EGF supplementation. (A) Growth efficiency of single CD326$^+$CD44$^+$ cells isolated at 7 d from *Gpr182$^{+/+}$; CMV-Cre* and *Gpr182$^{\Delta/\Delta}$; CMV-Cre* jejunum. Following 2 d in culture EGF was either supplemented (solid bars) or excluded (striped bars). One thousand CD326$^+$CD44$^+$ cells were initially plated in triplicate per mouse. **(B)** Growth efficiency at 7 d as a percent change compared to normalized EGF supplemented CD326$^+$CD44$^+$ cells. **(C)** Representative images of organoids following 7 d in culture (5d without EGF supplementation). **(D)** Relative expression of *Egfr* of whole jejunum from *Gpr182$^{+/+}$; CMV-Cre* and *Gpr182$^{\Delta/\Delta}$; CMV-Cre* mice and 5 d post-IRR *Gpr182$^{+/+}$* and *Gpr182$^{lacZ/lacZ}$* jejunum. Expression was normalized to *Gpr182$^{+/+}$; CMV-Cre and 18S*. Scale bars represent 500 μm. Biological n = 3 mice. Significance was determined by 1-way ANOVA with Tukey's Multiple Comparison Test.

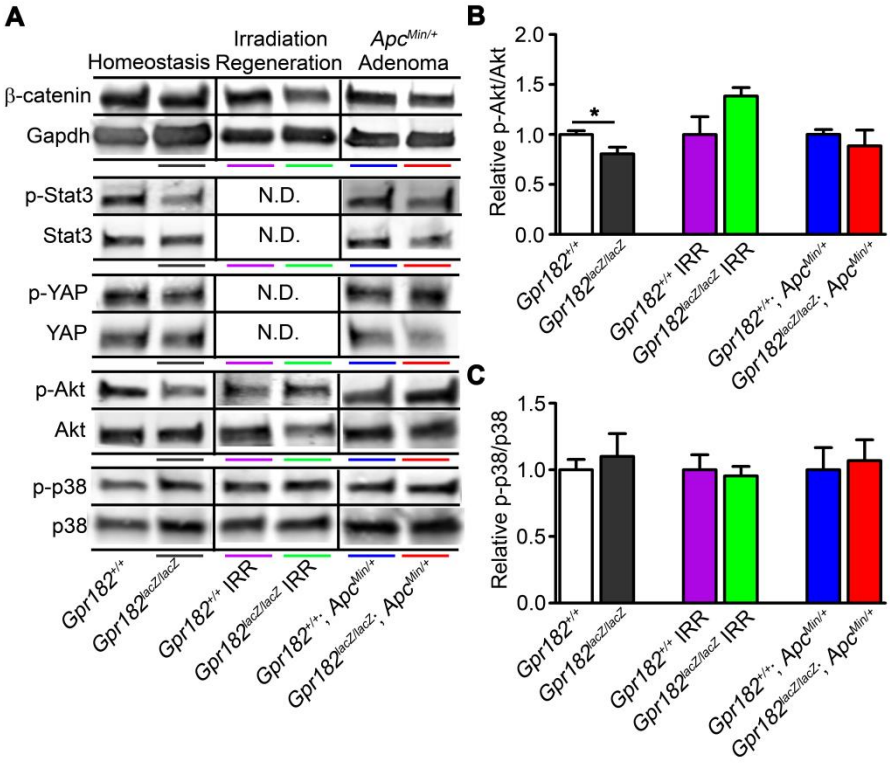

Supplemental Figure 8: *Gpr182* knockdown does not alter signaling through p38 MAPK, Akt, YAP, or Stat3. (A) Representative immunoblots of relative β-catenin and phosphorylated p38, Akt, YAP, and Stat3 between *Gpr182*$^{+/+}$ and *Gpr182*$^{lacZ/lacZ}$ from unchallenged, 5 d post-IRR, and *Apc*$^{Min/+}$ polyps of whole jejunum. Samples were normalized to Gapdh, total p38, Akt, YAP, Stat3 and *Gpr182*$^{+/+}$. Quantification of relative phosphorylated **(B)** Akt and **(C)** p38 normalized to total Akt or p38. n = 3-10 mice per genotype per condition. Significance was determined by unpaired T-test.

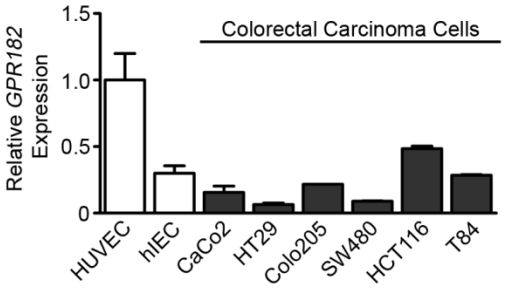

Supplemental Figure 9: Low *GPR182* expression in human colorectal cell lines. Relative *GPR182* expression in human cell lines, including a panel of colorectal carcinoma cell lines, intestinal epithelial cell (hIEC), and HUVECs. Expression was normalized to HUVECs and *GAPDH*. n = 2-4 per cell line.

Allele	Forward Primer (5' – 3')	Reverse Primer (5' – 3')	Taqman Probe
***Gpr182* Wild-type**	CTGCAGCCTCCTGGCACTAACAGC	CATTGTCCGGTTCCAAGGTGGAGAC	
***Gpr182*$^{tm2a(KOMP)Wtsi}$ Targeted**	GAGATGGCGCAACGCAATTAAT	GGGAGGATACCACAGGGAAATAGAGC	
***Gpr182 lacZ* Targeted**	TTCACTGGCCGTCGTTTTACAACGT	ATGTGAGCGAGTAACAACCCGTCGGATTCT	
***Apc* Wild-type**	GCCATCCCTTCACGTTAG	TTCCACTTTGGCATAAGGC	
Apc Min Allele	TTCTGAGAAAGACAGAAGTTA	TTCCACTTTGGCATAAGGC	
mouse *Gpr182 (Admr)*			Mm01946034_s1
mouse *Lgr5*			Mm00438890_m1
mouse *Olfm4*			Mm01320260_m1
mouse *Bmi1*			Mm00776122_g1
mouse *Lrig1*			Mm00456116_m1
mouse *Tert*			Mm00436931_m1
mouse *Egfr*			Mm01187858_m1
mouse *Ccnd1*			Mm00432359_m1
mouse *Hes1*			Mm01342805_m1
mouse *Chga*			Mm00514341_m1
mouse *Lyz2*			Mm01612741_m1
mouse *18S*			Mm03928990_g1
mouse *β-actin*			Mm02619580_g1
mouse *Gapdh*			Mm99999915_g1
human *GPR182*			Hm01922099_s1
human *GAPDH*			4310884E

Supplemental Table 1: RT-PCR and Genotyping Primers and Probes. All Taqman probes were from Thermo Fisher Scientific or Applied Biosystems.